Proximity Injection of Plasticizing Molecules to Self-Assembling Polymers for Large-Area, Ultrafast Nanopatterning in the Sub-10-nm Regime

Jae Won Jeong,[†] Yoon Hyung Hur,[†] Hyeong-jun Kim,[‡] Jong Min Kim,[†] Woon Ik Park,[†] Mi Jeong Kim,[§] Bumjoon J. Kim,[‡] and Yeon Sik Jung[†,*]

[†]Department of Materials Science and Engineering, Korea Advanced Institute of Science and Technology (KAIST), 291 Daehak-ro, Yuseong-gu, Daejeon 302-701, Republic of Korea, [‡]Department of Chemical & Biomolecular Engineering, Korea Advanced Institute of Science and Technology (KAIST), 291 Daehak-ro, Yuseong-gu, Daejeon 302-701, Republic of Korea, and [§]Samsung Advanced Institute of Technology (SAIT), Mt. 14-1, Nongseo-dong, Giheung-gu, Yongin-si, Gyeonggi-do, 446-712, Republic of Korea

ABSTRACT While the uses of block copolymers (BCPs) with a high Flory–Huggins interaction parameter (χ) are advantageous for the improvement of resolution and line edge fluctuations of self-assembled nanoscale patterns, their slow chain diffusion results in a prolonged assembly time. Although solvent vapor annealing has shown great effectiveness in promoting the self-assembly of such BCPs, a practical methodology to achieve a uniform swelling level in wafer-scale BCP thin films has not been reported. Here, we show that a solvent-swollen polymer gel pad can be used as a highly controllable vapor source for the rapid, large-area (>200 mm in diameter) formation of sub-10-nm patterns from a high-χ BCP. The proximal injection of solvent vapors to BCP films and the systematic control of the swelling levels and temperatures can significantly boost the self-assembly kinetics, realizing the formation of well-aligned sub-10-nm half-pitch patterns within 1 min of self-assembly. Moreover, we show that the gel pad can be used for the shear-induced alignment of BCP microdomains in an extremely short time of ~5 s as well as for the generation of three-dimensional crossed-wire nanostructures with controlled alignment angles.

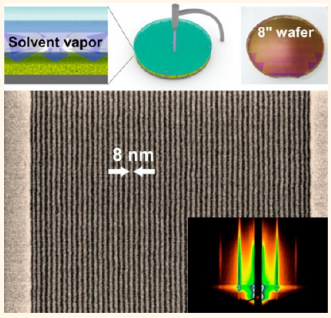

KEYWORDS: block copolymers · self-assembly · polydimethylsiloxane · polymer gel · solvent annealing

The directed self-assembly (DSA) of block copolymers (BCPs) is receiving growing attention from integrated circuit (IC) and information-storage industries mainly due to the excellent pattern resolution, cost-effectiveness, and high throughput.[1−14] Self-assembled nanoscale patterns derived from various BCPs composed of mutually incompatible polymer blocks have shown excellent ordering characteristics with dimensions in the range of 5 to 20 nm, which is well below the resolution limit of conventional photolithography.[15−19] The self-assembly of BCPs is driven by the minimization of the total free energy, which is composed of the strain energy and the interfacial/surface energy, *via* the spontaneous diffusion and rearrangement of the polymer chains.[20,21] Thus, the attainment of sufficient diffusivity is required for the accomplishment of well-ordered morphologies within a practical time scale. BCP chain mobility can be significantly enhanced by two distinct annealing methods: thermal annealing and solvent vapor annealing. Thermal annealing is performed by elevating the self-assembly temperature above the glass transition temperatures (T_g) of the constituent polymer blocks and has been adopted as the most common treatment method for DSA due to its simplicity.[1,4,5,22] Recently, the successful implementation of DSA on a 300 mm wafer was demonstrated using a thermal treatment on a poly(styrene-*b*-methylmethacrylate) (PS-PMMA) BCP.[16,17,23,24] On the other hand, solvent vapor annealing can plasticize BCPs by exposing them to solvent vapors, thus reducing the effective T_g below room temperature (RT),[25,26] which will be discussed in detail later in this article.

According to recent studies, including our previous reports, a BCP material with a relatively large Flory–Huggins interaction

* Address correspondence to ysjung@kaist.ac.kr.

Received for review April 1, 2013 and accepted July 1, 2013.

Published online July 01, 2013
10.1021/nn401611z

© 2013 American Chemical Society

parameter (χ) is advantageous for the improvement of the pattern resolution.[10,12−14] Sub-10-nm pattern formation results have been demonstrated using various high-χ BCPs such as poly(styrene-*b*-ethylene oxide) (PS-*b*-PEO),[13] poly(styrene-*b*-dimethylsiloxane) (PS-PDMS),[27,28] poly(2-vinylpyridine-*b*-dimethylsiloxane) (P2VP-PDMS),[29] polyhedral oligomeric silsesquioxane (POSS)-containing BCPs,[30,31] poly(*N*-xyloglucooligosaccharide-*b*-*para*-trimethylsilylstyrene) (XGO-PTMSS),[32] and poly(trimethylsilylstyrene-*b*-D,L-lactide) (PTMSS-PLA).[13] Moreover, the accomplishment of low line edge roughness (LER) requires the use of new BCPs with a much larger χ parameter.[33] However, the interdiffusivity of BCPs decreases exponentially with χ; as a result, high-χ BCPs have slower kinetics during the self-assembly process,[34] detrimentally affecting the throughput during pattern formation. For such high-χ BCPs, thermal annealing alone typically fails to obtain well-ordered structures within a reasonable time.[29,35,36]

On the other hand, solvent vapor annealing at RT has been more effective for the assembly of high-χ BCPs by demonstrating nanoscale morphologies with extensive long-range ordering.[10,28,37] Moreover, the wide controllability of the dimensions and orientation was demonstrated by the appropriate choices of solvents, swelling levels, and solvent compositions.[29,36,38] Recently, for the kinetic acceleration of BCP pattern formation, the combination of thermal annealing and solvent vapor annealing has also been demonstrated.[35,39] However, whether solvent vapor or solvothermal annealing is compatible with IC production in terms of scalability and large-area capability remains unanswered.[6] Moreover, precise control of the BCP swelling ratio (SR) is important because an excessively high SR can cause the dewetting of BCPs, while a low SR cannot effectively promote self-assembly. Previous studies performed solvent vapor annealing in a chamber containing solvent as a liquid source for the generation of vapors.[28,40−43] In such a system, the maintenance of a constant SR independently of the sample position is not simple because the distance between the vapor source (liquid) and the location on a wafer can vary, especially for large-area substrates. A chamber with a continuous flow of carrier gas containing solvent vapors generated from bubblers can provide more extensive controllability during solvent vapor annealing. However, in general, this type of chamber-based solvent vapor treatment requires initial stabilization time (~10 min) until the solvent vapor pressure in the chamber is saturated.[41,43] Moreover, to the best of our knowledge, no study has yet shown that wafer-scale, sub-10-nm DSA can be realized using solvent vapor annealing based on a simple, low-cost, and controllable configuration.

Here, we introduce a novel and practical approach involving the use of a solvent-saturated polymer gel pad as an extensively controllable vapor source for the large-area and chamber-free self-assembly of high-χ BCPs. We report that solvent-swollen polymer gel pads emit high-flux solvent vapors that can be directly injected into BCP thin films for the very effective facilitation of the self-assembly process. This strategy has multiple advantages that simplify solvent vapor annealing to scale up the DSA using high-χ BCPs. First, this method does not require chamber-based equipment with complicated vapor generation and delivery systems. Second, the small distance (~1 mm in this study) between the vapor source (gel pad) and the BCP thin films facilitates the very rapid swelling of BCPs. As a result, the nearly instantaneous stabilization of the swelling level in a BCP thin film is possible. Consequently, the self-assembly time is significantly shortened. Third, by adjusting the equilibrium vapor pressure of the gel pad, we can precisely and extensively control the swelling level of BCPs. This capability is important because the optimum swelling level depends on the BCPs, their molecular weights (MWs), incorporated solvents, and treatment temperature. Fourth, the independent control of the temperatures of the gel pad and the BCP samples enables the facile and significant acceleration of self-assembly kinetics. By exploiting these manifold advantages and with elaborate control of the self-assembly parameters, we demonstrate that the formation of self-assembled patterns with sub-10-nm resolutions can be uniformly induced on wafer substrates with a short assembly time (<1 min). In addition, we show that the direct contact of the polymer gel pad onto a BCP sample and the application of mild shear force can achieve the alignment of BCP microdomains without the requirement of a guiding template in an extremely short assembly time (~5 s).

RESULTS AND DISCUSSION

Figure 1 presents schematic diagrams and photographs describing the large-area DSA procedure using a polymer gel pad. It is well known that cross-linked polymers such as polydimethylsiloxane (PDMS) and hydrogels can effectively absorb solvent molecules in polymer networks. However, when such solvent-swollen gels are exposed to dry air, they gradually release the incorporated molecules and generate solvent vapors,[44−47] which was utilized for the self-assembly of BCPs in this study. A PDMS pad with a uniform thickness of 15 mm was prepared by pouring prepolymers and curing agents on a silicon substrate, which was followed by a subsequent thermal curing step. The flat polymer pad was put into a bath of solvents such as toluene, acetone, or a mixture of solvents. A fully swollen PDMS gel pad was then used for the annealing of various BCP films. In this study, PS-PDMS, an example of a high-χ BCP, was used for the demonstrations of PDMS gel pad annealing. SD45 and SD16 denote cylinder-forming PS-PDMS BCPs with MWs of 45.5 and 16 kg/mol, respectively. These BCP films were

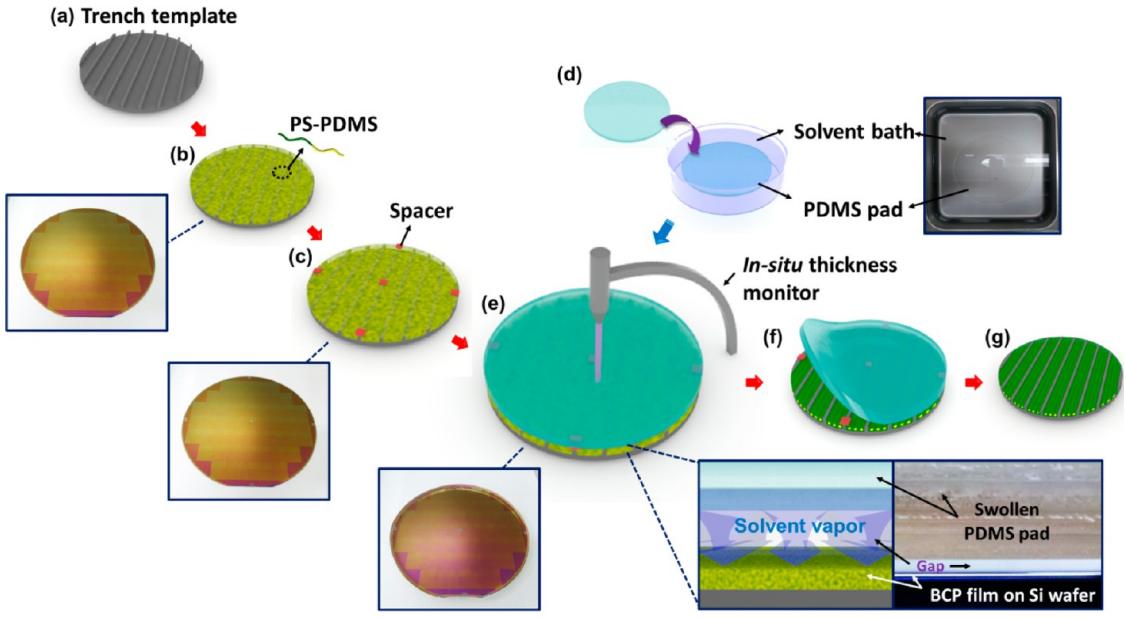

Figure 1. Procedure of large-area DSA using a solvent-saturated polymer gel pad. (a) Preparation of topographic guiding patterns by means of optical lithography. (b) Spin-casting of BCP. (c) Placement of 1-mm-thick spacers to control the gap distance. (d) Swelling of the PDMS pad in a solvent bath. (e) Proximity vapor annealing of BCP using the PDMS gel pad. The swelling ratio of the BCP film was monitored *in situ* using a spectroscopic reflectometer. (f) Rapid removal of the PDMS gel pad after the completion of the self-assembly process. (g) Reactive ion etching to obtain well-aligned SiO_x patterns.

spin-cast on PDMS-brush-coated silicon substrates from toluene solutions.[27] For the implementation of DSA, silicon substrates with surface trench patterns were used as guiding templates.[27,29] Small spacers with a height of 1 mm were placed on the substrates to maintain a constant gap (=1 mm) distance between the polymer pad and the BCP thin films. The swollen polymer gel pad placed on the sparse spacers (distance between the spacers ~100 mm) was rigid, such that the maximum change of gap distance in the intermediate regions between the spacers is approximately 3%. (See Figure S1 in the Supporting Information.) In order to initiate and facilitate the self-assembly process, a solvent-saturated PDMS gel pad was located on the spacers. After the completion of the self-assembly process, the self-assembled morphologies were quenched by the rapid removal of the PDMS pad, which was followed by two-step reactive ion etching with CF_4 and O_2 plasma to reveal the nanostructures.[8,27−29,35,38,48−50]

First, we measured the time-dependent mass increase of the PDMS pad when immersed in a toluene bath to investigate the incorporation dynamics of the solvent molecules into the cross-linked polymer pad. In Figure 2a, the mass swelling ratio, M/M_o, where M and M_o represent the masses of the swollen and dry pads, respectively, is plotted as a function of the square root of the immersion time ($t^{1/2}$). The linearity of the graphs during the initial swelling stage indicates that the penetration of the solvent molecules into the PDMS pad is a type of Fickian diffusion.[51] This occurs because polymer (PDMS) chain relaxation is faster than solvent diffusion,[51,52] which is consistent with the fact that the glass transition temperature ($T_g = -125$ °C)[53] of PDMS is significantly lower than the solvent incorporation temperatures ($T_i = 25$, 60, and 80 °C). A higher T_i, where solvent diffusion is faster, achieved a fully saturated gel state in a much shorter time, as shown in Figure 2a. The saturated mass swelling ratios (M_s/M_o) were 1.96, 2.01, and 2.03 for T_i = 25, 60, and 80 °C, respectively. The slightly higher M_s/M_o at a higher T_i can be attributed to the decrease of the interaction parameter (χ) between the PDMS and toluene, allowing a higher fraction of solvents in the cross-linked polymer chain. Despite the large mass loading in the cross-linked PDMS, the gel pad maintained its flatness without any distortion, which is beneficial for the maintenance of a gap with a constant distance between the pad and the BCP film during self-assembly.

For the swelling of a cross-linked polymer network in a pure solvent, the difference between the chemical potential ($\mu_{s,pad}$) of the solvent molecules in the polymer network and that (μ_s^o) of the molecules in the surrounding liquid is associated with the elastic free energy and mixing free energy. It can be expressed using the following equation:[46]

$$\Delta\mu_s = \mu_{s,\,pad} - \mu_s^o = RT_i \ln(P_x/P_o) = GV_s\left[(\phi_{PDMS})^{1/3} - (\phi_{PDMS})\right] + RT_i[\ln(1-\phi_{PDMS}) + \phi_{PDMS} + \chi\phi_{PDMS}{}^2] \quad (1)$$

Here, P_x is the vapor pressure of the PDMS gel, P_o is the equilibrium vapor pressure of the liquid surrounding the PDMS gel, R is the gas constant, G is the elastic

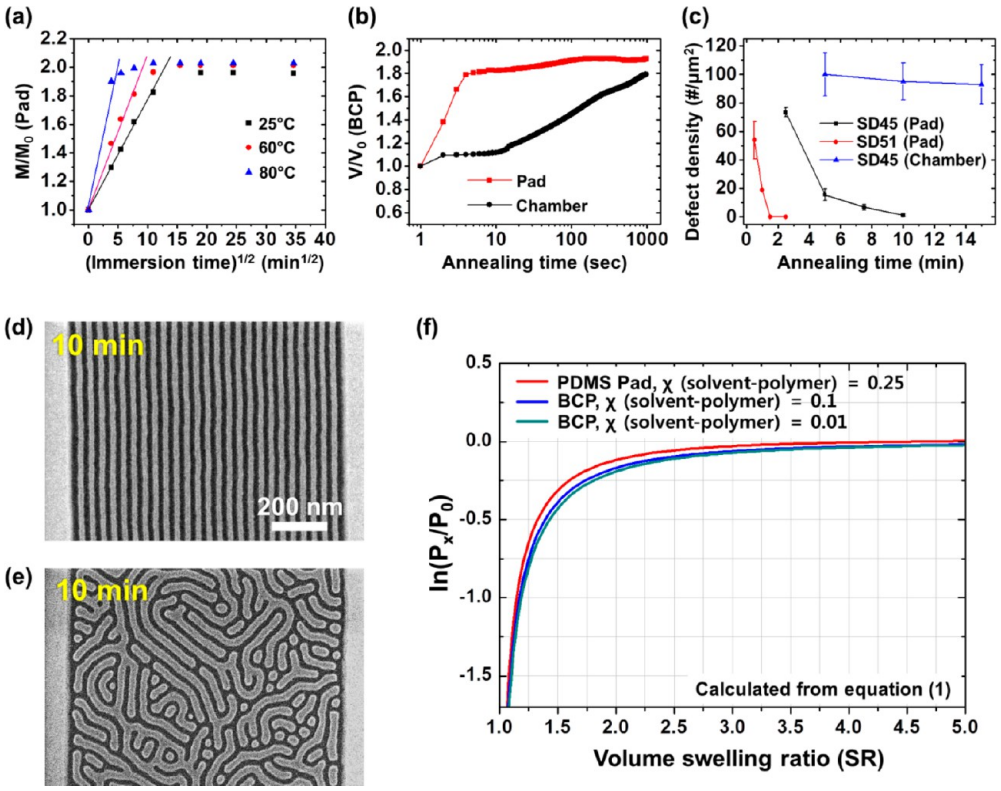

Figure 2. Swelling dynamics of the PDMS gel pad and BCP thin films. (a) Mass swelling ratio (M/M_o) of a PDMS gel pad *vs* the square root of the immersion time ($t^{1/2}$) in a toluene bath. (b) Time-dependent volume swelling ratio (V/V_o) of a SD45 BCP film. (Here, "pad" and "chamber" represent "pad annealing" and "conventional solvent annealing in a chamber system", respectively.) (c) Defect density decay of the BCP films as a function of the annealing time. (d, e) Surface morphologies of SD45 BCP films annealed for 10 min using (d) the swollen PDMS pad and (e) a conventional chamber containing a liquid solvent as a vapor source. SEM images at a lower magnification level are shown in Figure S5. (f) Plots of the relative partial pressure ($\ln(P_x/P_o)$) of the gel pad and BCP films as a function of SR (calculated from eq 1).

modulus of the PDMS, V_s is the molar volume of the solvent, and ϕ_{PDMS} is the volume fraction of the PDMS in the PDMS-solvent gel. In a fully saturated state, a dynamic equilibrium is achieved, leading to

$$\Delta\mu_s = \mu_{s,\,pad} - \mu_s^o = RT_i \ln(P_x/P_o) = 0 \rightarrow P_x = P_o \quad (2)$$

Therefore, like a pure liquid, the solvent-saturated PDMS gel pad can also emit high-flux vapors into the surrounding gas phase (air); the vaporized solvent molecules are rapidly absorbed by the BCP films placed at a proximal distance of 1 mm. As shown in Figure 2b, the increase of the volume swelling ratio (V/V_o) of the BCP film (SD45) annealed by the PDMS gel pad arrives at the saturation point SR (~1.93) within 5 s, which can be attributed to the very short diffusion distance (~gap distance) of the solvent molecules. The details on SR measurement are shown in Figure S2 in the Supporting Information. In contrast, chamber annealing requires a much longer ramp time (>15 min), which is consistent with previous studies.[41,43] Such rapid swelling dynamics even at room temperature enables fast decay of the defect density and the uniform alignment of a cylinder-forming SD45 BCP film in 1-μm-wide trenches within an annealing time of 10 min (Figure 2c and d) as well as a sphere-forming SD51 BCP film (Figures 2c and S3). In contrast, the chamber annealing could not complete the assembly process even after 15 min (Figure 2c and e). Similarly, proximity annealing using a liquid source (toluene) instead of a polymer gel also achieved rapid self-assembly (Figure S4). However, a critical issue pertaining to the liquid-state source is the significant height fluctuation of its surface. The application of slight vibrations on the liquid significantly changes the gap distance or even damages the BCP films due to the direct contact between the liquid and the BCP. In contrast, a polymer gel pad can emit high-flux vapors without such issues owing to its sufficient rigidity and solidness.

While such a high SR (~2) is advantageous for the self-assembly of larger-MW BCPs forming patterns with relatively low densities (full pitch >30 nm), the formation of sub-10-nm half-pitch patterns requires a BCP with a smaller MW and a lower SR.[28,36] Thus, the attainment of the capability to control the BCP swelling level is critical for feature size modulation in a wide range. To achieve this, we developed a facile means of controlling the swelling level of the PDMS pad by immersing it in mixed solvents of toluene and acetone with different compositions. Because acetone cannot effectively

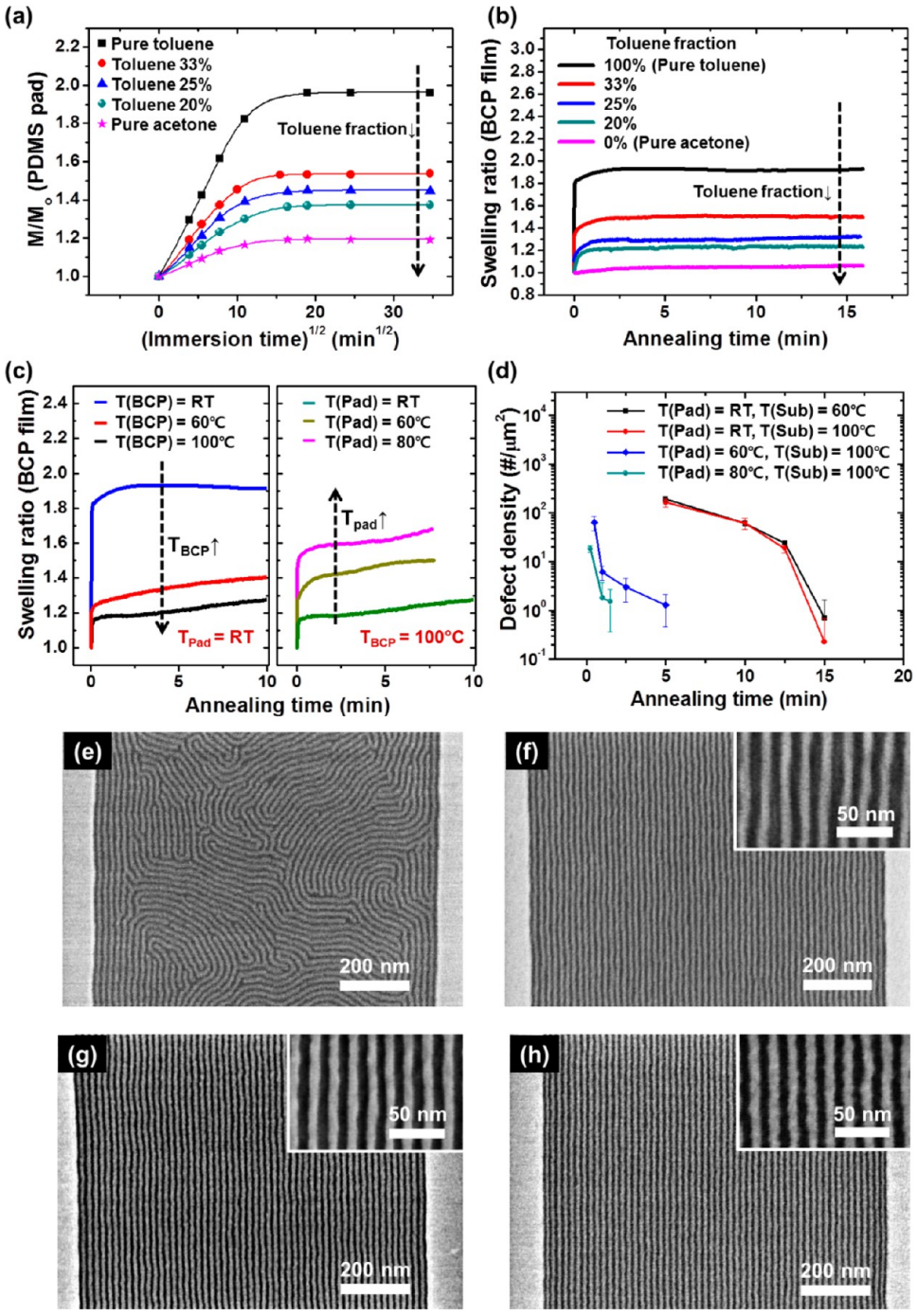

Figure 3. Systematic control of the kinetics of BCP self-assembly. (a) Mass swelling ratio (M/M_o) of a PDMS gel pad *vs* the square root of the immersion time ($t^{1/2}$) in mixed solvents of toluene and acetone. (Percentages denote the volume fraction of toluene.) (b, c) Time-dependent volume SR of SD45 (MW = 45.5 kg/mol) BCP films depending on (b) the mixing ratio of the solvent bath and (c) the temperatures of the PDMS pad (T_{Pad}) and BCP film (T_{BCP}). (d) Defect density of line/space patterns from SD16 BCP *vs* the annealing time using the gel pad. (e–h) Morphologies of the SD16 BCP (MW = 16 kg/mol) after the self-assembly process and plasma oxidation: (e) Vapor source: toluene-saturated PDMS pad, $T_{Pad} = T_{BCP}$ = RT, annealing time = 30 s. A longer annealing time caused the dewetting of the BCP film, as shown in Figure S6. (f) Vapor source: PDMS pad immersed in a mixed solvent of toluene and acetone (1:3), $T_{Pad} = T_{BCP}$ = RT, annealing time = 15 min. (g) Vapor source: toluene-saturated PDMS pad, T_{Pad} = RT, T_{BCP} = 60 °C, annealing time = 15 min. (h) Vapor source: toluene-saturated PDMS pad, T_{Pad} = 80 °C, T_{BCP} = 100 °C, annealing time = 1 min.

penetrate into the PDMS chain network compared to toluene due to the larger interaction parameter (χ) between acetone and PDMS compared to that between toluene and PDMS, the equilibrium mass SR of PDMS is determined by the solvent mixing ratio, as shown in Figure 3a. In turn, the SR determines the equilibrium partial pressure of the vapor emitted by the swollen PDMS pad. The decreased mass SR of the

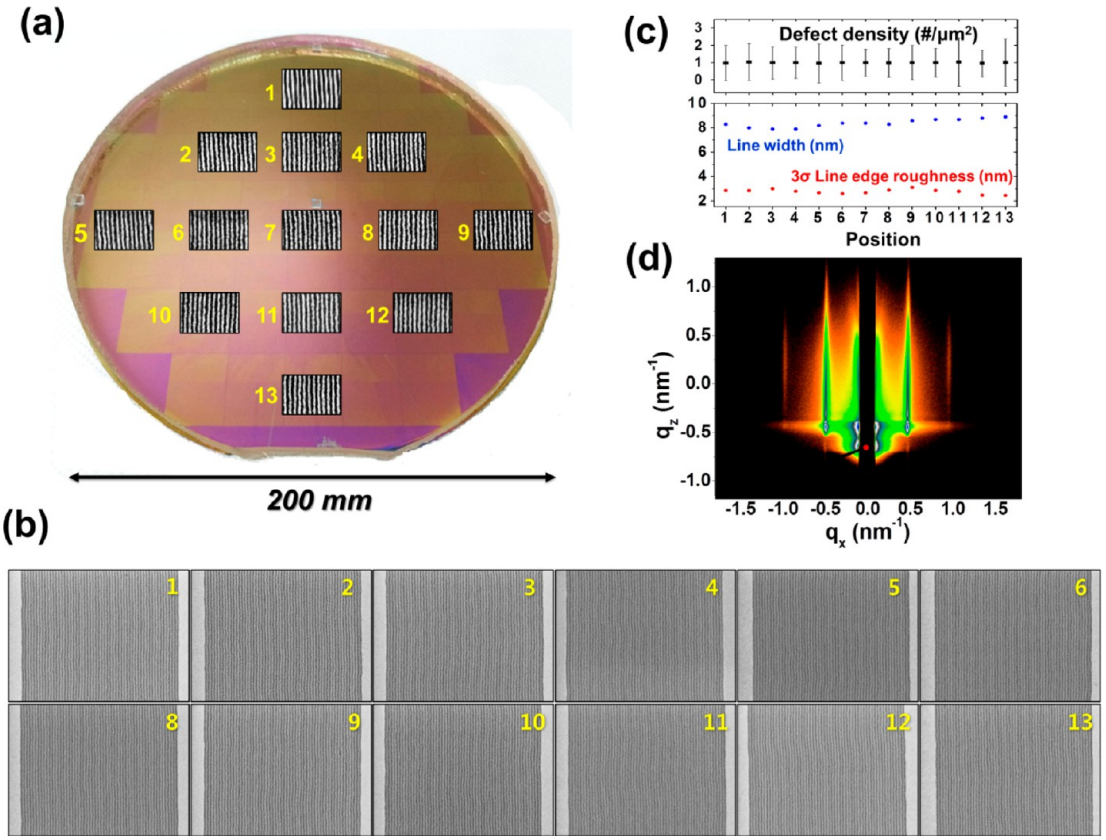

Figure 4. Demonstration of 8-nm-wide patterns on a large-area substrate. (a) Photograph of a SD16 BCP-coated 200-mm wafer under a transparent PDMS gel pad overlapped with high-magnification SEM images of the line/space patterns. The samples were collected from 13 selected locations on the wafer. (b) Low-magnification SEM images of the line/space patterns. (c) Distribution of the defect density, line width, and 3σ line edge roughness depending on the location on the wafer. (d) GISAXS pattern of the sample collected from the center of the wafer.

PDMS pad with an increase in the acetone fraction in the solvent mixture lowers the equilibrium vapor pressure, as presented in the graphs shown in Figure 2f. The equilibrium toluene vapor pressure of the PDMS gel pad (saturated by the mixed solvents) can be expressed as $P_x = \alpha P_o (0 \leq \alpha \leq 1)$, where α (=the activity of toluene in the gel) is controlled by the solvent mixing ratio. This controllable vapor pressure of the PDMS gel pad can be confirmed by the decreasing trend of the BCP SR value from 1.93 to 1.06 as the fraction of toluene in the solvent mixture is reduced from 1.0 to 0 (Figure 3b). For the swelling of BCP films, the elastic free energy can be ignored, and eq 1 is simplified to

$$\begin{aligned} \Delta\mu_s &= \mu_{s,\,BCP} - \mu_s^o = RT_{BCP}\ln(P_x/P_o) \\ &= RT_{BCP}[\ln(1-\phi_{BCP}) + \phi_{BCP} + \chi\phi_{BCP}^2] \end{aligned} \quad (3)$$

where P_x is the vapor pressure of the solvent vapor generated by the PDMS gel pad and ϕ_{BCP} (=1/SR) is the fraction of BCP in the swollen state. Thus, P_x in the vapor phase surrounding the BCP films directly controls the SR values. This equation is also plotted in Figure 2f. Although both the high SR of 1.93 and the low SR of 1.06 could not induce the uniform ordering of the SD16 BCP in 1-μm-wide trenches, as shown in Figures 3e and Figure S7, respectively, the optimized SR of 1.32 could achieve a good ordering (Figure 3f and Figure S8, annealing time = 15 min).

Another strong advantage of proximity vapor annealing using a polymer gel pad is that the temperatures of the vapor source (pad) and BCP films can be independently controlled. These temperature modulations significantly affect the SR of BCP films and consequently the self-assembly kinetics. For example, we observed that the SR decreases as T_{BCP} is increased while fixing T_{Pad}, as shown in Figure 3c (left-hand side). This phenomenon can be understood by the analytical equations 1−3. At a higher T_{BCP}, P_x/P_o is significantly decreased due to the exponential increase of $P_o \approx \exp(-(\Delta H_{vap}/RT_{BCP}))$ with T_{BCP}, where ΔH_{vap} is the enthalpy of evaporation for liquid toluene. In contrast, P_x is solely determined by the equilibrium vapor source of the PDMS gel pad and remains constant at the same T_{Pad}. Thus, from eq 3 and Figure 2f, a higher T_{BCP} leads to a reduced SR (increased ϕ_{BCP}), which is consistent with the trend in Figure 3c (left-hand side). Similarly, while fixing T_{BCP}, T_{Pad} was independently increased to monitor the changes in the SR of BCP film. T_{Pad} during proximity vapor annealing was identical to the temperature of the solvents that swelled the PDMS pad. In the fully swollen state, $P_x = P_o \approx \exp(-(\Delta H_{vap}/RT_{Pad}))$

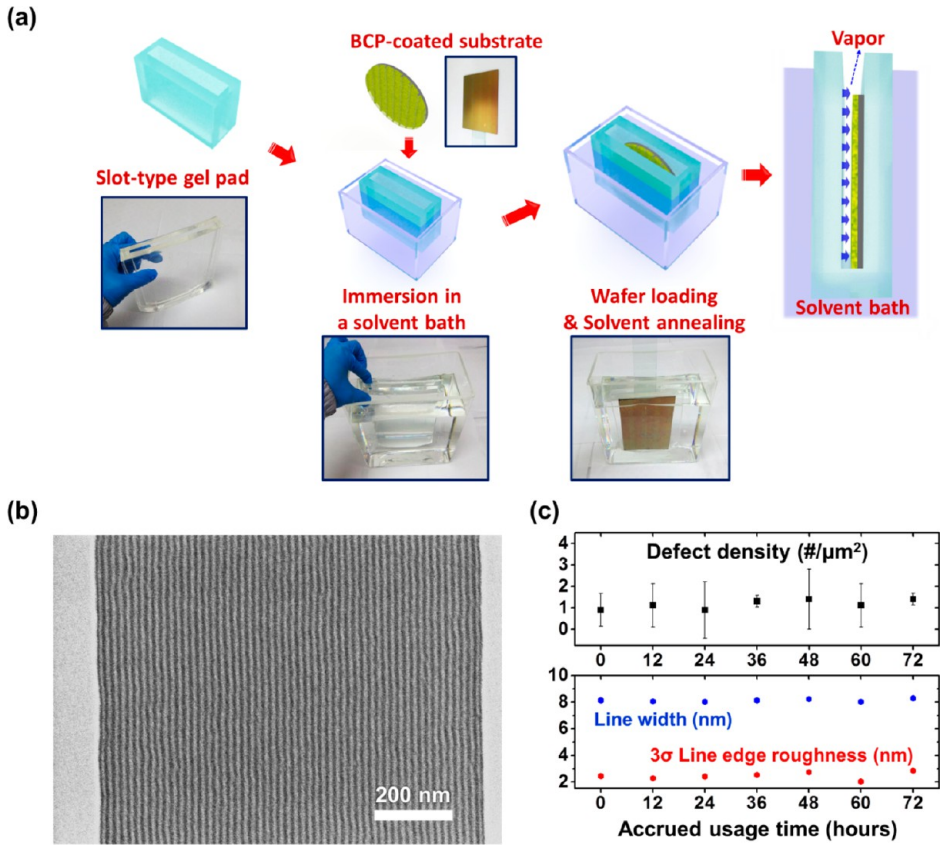

Figure 5. Slot-type hollow gel pad for continuous usage. (a) Schematic diagram and photographs describing the procedure of proximity solvent annealing using a hollow gel pad (wafer size: 14 cm × 10 cm). (b) Self-assembled morphology of a cylinder-forming SD16 BCP (MW = 16 kg/mol) film annealed for 30 min (accrued usage time of the pad = 72 h in a mixed solvent of toluene/acetone (1:3, by volume)). (c) Variations of defect density, line width, and 3σ line edge roughness depending on accumulated usage time of the gel pad.

according to eq 2; consequently, P_x around the BCP film increases exponentially with T_{Pad}. As a result, the SR of the BCP films increased with an increase in T_{Pad}, as indicated in Figure 3c (right-hand side). However, when T_{sub} is lower than T_{pad}, the solvent vapor in the gap space can condense to liquid on the surface of BCP films. Thus, in order to prevent such undesirable solvent condensation, the pad annealing was performed while maintaining the condition of $T_{sub} \geq T_{pad}$.

By exploiting the extensive SR controllability *via* temperature modulations, we could successfully and uniformly assemble the SD16 BCP using a PDMS pad saturated with pure toluene, as shown in Figure 3g. (Figure S9 shows the time-evolution results of the self-assembled patterns.) Moreover, as previously reported by the authors, thermal assistance during solvent vapor annealing can significantly accelerate the self-assembly kinetics of high-χ BCPs.[35] As shown in Figure 3d, the higher T_{BCP} and T_{Pad} values achieved a much faster decay of the defect density. Under an optimized condition, the self-assembly of BCPs in 1-μm-wide trenches was completed in 1 min, which is considerably shorter than the assembly time of 15 min for RT annealing (Figure 3f), as demonstrated in Figure 3d and h. Figure S10 also shows that well-aligned dot patterns from a sphere-forming BCP were successfully assembled in 15 s. The assembly time is expected to be further reduced by decreasing the trench width.[35]

We now demonstrate the large-area pattern formation capability using the polymer gel pad as a uniform vapor source. Cross-linked PDMS pads of 200 and 300 mm in diameters were put into a mixed solvent of toluene/acetone (1:3, by volume) at RT. A 200-mm-wide Si wafer with 1-μm-wide and 40-nm-deep topographic trench patterns was prepared using KrF optical lithography, and the wafer was coated with a PDMS brush layer. Figure 4a shows an optical image of the BCP-coated 200 mm wafer under a transparent PDMS gel pad ($T_{Pad} = T_{BCP}$ = RT). The measured SR of the BCP film was uniform across the entire wafer surface, which is also supported by the constant color of the BCP film. After the completion of the self-assembly process, 13 chip samples were collected for an analysis from different locations on the wafer. Their high-magnification SEM images are overlaid on the wafer's optical image in Figure 4a, while images taken at a lower magnification are shown in Figure 4b to demonstrate the uniform registration of the line patterns along the trench walls. Their defect density, line width, and line edge roughness were consistent in all 13 samples

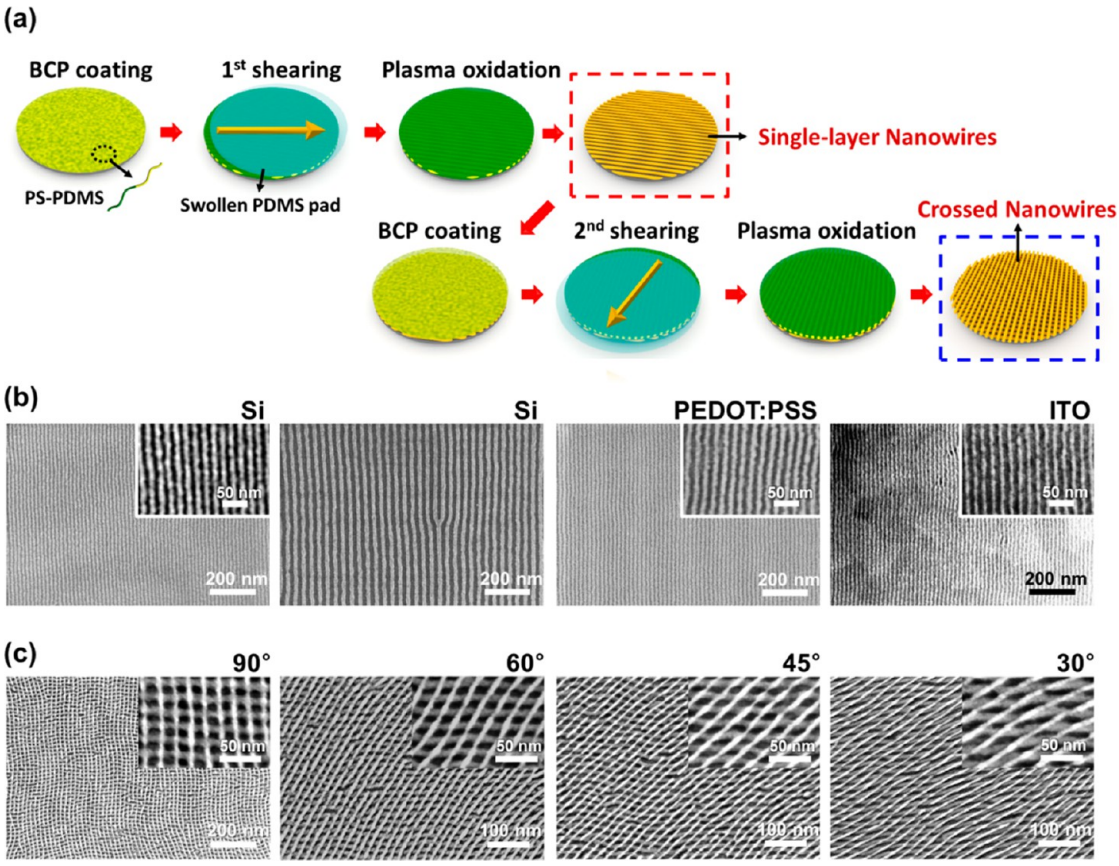

Figure 6. Ultrafast shear alignment using a gel pad. (a) Schematic diagram showing the procedures for the shear-induced alignment of BCP patterns using a solvent-swollen PDMS pad and the fabrication of crossed-wire structures *via* sequential shear alignment. The PDMS gel pad here is in a direct contact with the BCP film. (b) SEM images of the shear-aligned cylinders from SD16 and SD45 BCPs on a PS-brush-coated planar Si substrate, a poly(3,4-ethylenedioxythiophene):poly(styrenesulfonate) (PEDOT:PSS) thin film, and an indium tin oxide (ITO) thin film. The formation of well-aligned patterns was achieved within 5 s of contact time. (c) Crossed-wire structures with controlled alignment angles obtained by consecutive shear-induced alignment.

without significant amounts of variation (Figure 4c). For the calculation, we ignored the nonuniformity inevitably caused by dust particles due to the limited cleanliness of our clean room. The clearly resolved linear diffraction patterns in the grazing-incidence small-angle X-ray scattering (GISAXS) analysis data (Figure 4d) also support the good regularity of the self-assembled patterns over the macroscopic analysis area. We also confirmed that this gel pad annealing process can be effective for a 300-mm wafer by evenly distributing small BCP-coated chips on the large-area wafer, performing gel pad annealing, and then checking the self-assembly results (see Figure S11 in the Supporting Information).

The solvent-swollen polymer pad can provide a constant BCP SR for at least 60 min without being reimmersed in a solvent bath. However, as the pad discharges solvent vapors, the equilibrium vapor pressure of the gel pad gradually decreases, inevitably requiring the periodic and repetitive immersion of the PDMS pads. Thus, the continuous usage of the gel pad by a simple replenishment of solvents would simplify the process and increase the throughput of pattern formation. As shown in Figure 5a, this can be accomplished by employing a hollow gel pad, where a BCP-coated wafer can be mounted for annealing. By immersion in a solvent bath, the "slot-type" PDMS gel can always maintain equilibrium of the swelling state and the same vapor pressure in the internal gap region because, from the solvent reservoir, it can continuously receive as many molecules as are emitted to the vapor phase, maintaining its dynamic equilibrium state. As presented in Figures 5b and c, we confirmed that there is no detectable change in the self-assembled patterns. The line and space patterns obtained by the continuous usage of the hollow gel pad for 72 h showed the maximum variation of the average line width of less than 12%.

In addition to the PS-PDMS BCPs, the PDMS gel pad can also induce self-assembled polystyrene-*b*-poly(2-vinylpyridine) (PS-P2VP) BCP, as shown in Figure S12. However, for more extensive usability of gel pad vapor annealing for various BCPs, we can consider other cross-linkable polymers such as polytetrafluoroethylene, polybutadiene, polystyrene, polyurethane acrylate, polyvinyl alcohol, polyethylene oxide (PEO), and even gelatin and fabric that can absorb from extremely hydrophobic to hydrophilic solvents and can gradually

emit their vapors. As an example, the self-assembly of poly(2-vinylpyridine-*b*-dimethylsiloxane) was successfully performed using a thick fabric pad saturated with isopropyl alcohol, as presented in Figure S12. In addition, a hydrogel pad that can produce high-flux water vapor[54] is shown in Figure S13.

Finally, we demonstrate that the solvent-swollen pad can be utilized for the ultrafast shear alignment of BCP thin films. The advantage of this method arises from its simplicity because it does not require guiding templates such as trenches or chemical surface patterns for the long-range ordering of BCP microdomains.[55−57] In our approach shown in Figure 6a (detailed configurations are shown in Figure S14), the solvent-containing PDMS pad effectively plasticizes the BCP film in contact with the pad and enables the completion of shear alignment in a time of 5−30 s, which is significantly shorter than that in previous studies.[56] Shear alignment with a shear speed of 10 μm/s and an applied pressure of 50 kPa was performed immediately after the attachment of the toluene-saturated PDMS pad on a BCP sample. Figure 6b and Figure S15 illustrate how single-layer silica nanowire patterns are uniformly formed on surfaces including bare Si, poly(3,4-ethylenedioxythiophene):poly(styrenesulfonate) thin film, and indium tin oxide thin film without a guiding template or surface treatment. Moreover, the sequential shear alignment realized the formation of three-dimensionally crossed nanowires with controlled alignment angles, as shown in Figure 6c and Figure S16. Despite the relatively higher defect density compared to assembled patterns guided by templates (as shown in Figure S17), this technique greatly simplifies the formation of ultrasmall nanostructures and the control of their orientations.

CONCLUSIONS

We demonstrated the novel application of a solvent-swollen polymer gel pad as an extensively controllable solvent source for the ultrafast, large-area, high-resolution pattern formation from a high-χ BCP. The extremely fast self-assembly kinetics was achieved by the proximal injection of solvent vapors to BCP films using the polymer gel pads and by the systematic control of the swelling ratios of BCPs and the temperatures of the gel pad and BCP thin films. This study also revealed that the solvent-emitting gel pad can be used for the shear-induced alignment of BCP nanostructures in an extremely short time of <5 s. Moreover, the construction of three-dimensional crossed-wire nanostructures with controlled alignment angles was successfully demonstrated. We expect that this facile and versatile proximity solvent vapor annealing method using a solvent-swollen polymer gel pad will be very practical when used for high-density pattern formation with high-χ BCPs due to the ultrafast assembly kinetics and greater simplicity. Moreover, this technique can be extended beyond the DSA of BCPs to a variety of other areas, such as organic photovoltaics for the formation of improved bulk heterojunctions[58] or for plasmonic nanocrystal self-organization,[59] where a simpler, faster, and large-area solvent vapor treatment can be highly beneficial.

METHODS

Fabrication of PDMS Gel Pads. Prepolymers and curing agent (Sylgard 184, Dow Corning Co. Ltd.) were mixed with a weight ratio of 10:1, and the resultant air bubbles in the mixture were eliminated by degassing under vacuum. The mixture was then poured onto a silicon wafer and baked at 140 °C for 30 min using a convection oven. The prepared PDMS samples with a thickness of 15 mm were immersed into a bath of solvent such as toluene, acetone, or a mixture of solvents for the preparation of gel pads. The fully swollen PDMS pads were taken out from the solvent bath, and the solvent drops on the pads were immediately eliminated by gently blowing them with nitrogen gas for 30 s.

Fabrication of Si Trench Templates. The Si trench templates for DSA were fabricated using KrF photolithography followed by reactive ion etching. A positive photoresist (PR, Dongjin Semichem Co. Ltd., Korea) with a thickness of 400 nm was spin-coated on 200 mm Si wafers. The PR film was then exposed to a KrF scanner (Nikon, NSR-S203B), which was followed by developing using a developer solution (tetramethylammonium hydroxide, Dongjin Semichem Co. Ltd.). The PR patterns were used as an etch mask to pattern the Si surface by reactive ion etching (gas: CF_4, working pressure: 7 mTorr, plasma power: 250 W). After the stripping of the remaining PR, trench patterns with a width of 1 μm, a depth of 40 nm, and a period of 1.25 μm were obtained and used for DSA.

BCPs and Other Polymers. All BCPs and end-functionalized polymers used in this study were purchased from Polymer Source Inc. (Canada). Cylinder-forming PS-PDMS BCPs with MWs of 45.5 kg/mol (SD45, f_{PDMS} = volume fraction of PDMS = 33.5%) and 16 kg/mol (SD16, f_{PDMS} = 32.9%) were used for the formation of line patterns. We also used sphere-forming PS-PDMS BCPs with MWs of 51.5 kg/mol (SD51, f_{PDMS} = 16.5%) and 28 kg/mol (SD28, f_{PDMS} = 11.5%). A PS-P2VP BCP with a MW of 34 kg/mol (f_{P2VP} = 29.6%) and a P2VP-PDMS BCP with a MW of 26 kg/mol (f_{PDMS} = 41.6%) were also used. Hydroxy-terminated PDMS homopolymers with a MW of 5 kg/mol were used for the surface modification of Si trench templates.

Pt Ion Incorporation. After the completion of gel pad annealing, PS-P2VP BCP films were dipped in a Pt-ion-containing solution for 30 min at RT. The solution was prepared by mixing a 10 mM Na_2PtCl_4 aqueous solution and 1% hydrochloric acid with a volume ratio of 1:9. The films were then washed with DI water and treated with O_2 plasma for 30 s using reactive ion etching.

Reactive Ion Etching of Self-Assembled BCP Samples. In order to remove the top-segregated PDMS layer and organic blocks (PS or P2VP), the samples were etched by CF_4 plasma (etching time = 20 s, gas flow rate = 30 sccm, working pressure = 15 mTorr, and plasma power = 60 W) followed by O_2 plasma (etching time = 30 s, gas flow rate = 30 sccm, working pressure = 15 mTorr, and plasma power = 50 W).

SEM Characterization and Image Analysis. For the observation and analysis of self-assembled patterns, a field emission scanning electron microscope (FE-SEM, Hitachi S-4800) with an acceleration voltage of 15 kV and a working distance of 5 mm was used. In order to quantify the line width, line edge roughness, and line width roughness, commercial image analysis software (SuMMIT) was used.

Conflict of Interest: The authors declare no competing financial interest.

Acknowledgment. This work was supported by the Center for Integrated Smart Sensors funded by the Ministry of Science,

ICT & Future Planning as Global Frontier Project (CISS-2012366054188), and by the Fundamental R&D Programs for Core Technology of Materials funded by Ministry of Trade, Industry & Energy of Korea (No. 10040038).

Supporting Information Available: Supplementary figures. This material is available free of charge *via* the Internet at http://pubs.acs.org.

REFERENCES AND NOTES

1. Park, M.; Harrison, C.; Chaikin, P. M.; Register, R. A.; Adamson, D. H. Block Copolymer Lithography: Periodic Arrays of Similar to 10(11) Holes in 1 Square Centimeter. *Science* **1997**, *276*, 1401–1404.
2. Rockford, L.; Liu, Y.; Mansky, P.; Russell, T. P.; Yoon, M.; Mochrie, S. G. J. Polymers on Nanoperiodic, Heterogeneous Surfaces. *Phys. Rev. Lett.* **1999**, *82*, 2602–2605.
3. Segalman, R. A.; Yokoyama, H.; Kramer, E. J. Graphoepitaxy of Spherical Domain Block Copolymer Films. *Adv. Mater.* **2001**, *13*, 1152–1155.
4. Kim, S. O.; Solak, H. H.; Stoykovich, M. P.; Ferrier, N. J.; de Pablo, J. J.; Nealey, P. F. Epitaxial Self-Assembly of Block Copolymers on Lithographically Defined Nanopatterned Substrates. *Nature* **2003**, *424*, 411–414.
5. Cheng, J. Y.; Mayes, A. M.; Ross, C. A. Nanostructure Engineering by Templated Self-Assembly of Block Copolymers. *Nat. Mater.* **2004**, *3*, 823–828.
6. Black, C. T.; Ruiz, R.; Breyta, G.; Cheng, J. Y.; Colburn, M. E.; Guarini, K. W.; Kim, H. C.; Zhang, Y. Polymer Self Assembly in Semiconductor Microelectronics. *IBM J. Res. Dev.* **2007**, *51*, 605–633.
7. Darling, S. B. Directing the Self-Assembly of Block Copolymers. *Prog. Polym. Sci.* **2007**, *32*, 1152–1204.
8. Bita, I.; Yang, J. K.; Jung, Y. S.; Ross, C. A.; Thomas, E. L.; Berggren, K. K. Graphoepitaxy of Self-Assembled Block Copolymers on Two-Dimensional Periodic Patterned Templates. *Science* **2008**, *321*, 939–943.
9. Ruiz, R.; Kang, H. M.; Detcheverry, F. A.; Dobisz, E.; Kercher, D. S.; Albrecht, T. R.; de Pablo, J. J.; Nealey, P. F. Density Multiplication and Improved Lithography by Directed Block Copolymer Assembly. *Science* **2008**, *321*, 936–939.
10. Park, S.; Lee, D. H.; Xu, J.; Kim, B.; Hong, S. W.; Jeong, U.; Xu, T.; Russell, T. P. Macroscopic 10-Terabit-per-Square-Inch Arrays from Block Copolymers with Lateral Order. *Science* **2009**, *323*, 1030–1033.
11. Yang, J. K. W.; Jung, Y. S.; Chang, J. B.; Mickiewicz, R. A.; Alexander-Katz, A.; Ross, C. A.; Berggren, K. K. Complex Self-Assembled Patterns Using Sparse Commensurate Templates with Locally Varying Motifs. *Nat. Nanotechnol.* **2010**, *5*, 256–260.
12. Tavakkoli, K. G. A.; Gotrik, K. W.; Hannon, A. F.; Alexander-Katz, A.; Ross, C. A.; Berggren, K. K. Templating Three-Dimensional Self-Assembled Structures in Bilayer Block Copolymer Films. *Science* **2012**, *336*, 1294–1298.
13. Bates, C. M.; Seshimo, T.; Maher, M. J.; Durand, W. J.; Cushen, J. D.; Dean, L. M.; Blachut, G.; Ellison, C. J.; Willson, C. G. Polarity-Switching Top Coats Enable Orientation of Sub-10-nm Block Copolymer Domains. *Science* **2012**, *338*, 775–779.
14. Chai, J.; Wang, D.; Fan, X.; Buriak, J. M. Assembly of Aligned Linear Metallic Patterns on Silicon. *Nat. Nanotechnol.* **2007**, *2*, 500–506.
15. Kim, H.-C.; Park, S.-M.; Hinsberg, W. D. Block Copolymer Based Nanostructures: Materials, Processes, and Applications to Electronics. *Chem. Rev.* **2009**, *110*, 146–177.
16. Bencher, C.; Yi, H.; Zhou, J.; Cai, M.; Smith, J.; Miao, L.; Montal, O.; Blitshtein, S.; Lavi, A.; Dotan, K.; *et al*. Directed Self-Assembly Defectivity Assessment. Part II. *Proc. SPIE* **2012**, *8323*, 83230N.
17. Liu, C.-C.; Pitera, J.; Lafferty, N.; Lai, K.; Rettner, C.; Tjio, M.; Arellano, N.; Cheng, J. Progress Towards the Integration of Optical Proximity Correction and Directed Self-Assembly of Block Copolymers with Graphoepitaxy. *Proc. SPIE* **2012**, *8323*, 83230X.
18. Tsai, H.-Y.; Miyazoe, H.; Engelmann, S.; To, B.; Sikorski, E.; Bucchignano, J.; Klaus, D.; Liu, C.-C.; Cheng, J.; Sanders, D.; *et al*. Sub-30 nm Pitch Line-Space Patterning of Semiconductor and Dielectric Materials Using Directed Self-Assembly. *J. Vac. Sci. Technol., B* **2012**, *30*, 06F205.
19. Peng, Q.; Tseng, Y.-C.; Darling, S. B.; Elam, J. W. A Route to Nanoscopic Materials *via* Sequential Infiltration Synthesis on Block Copolymer Templates. *ACS Nano* **2011**, *5*, 4600–4606.
20. Leibler, L. Theory of Microphase Separation in Block Copolymers. *Macromolecules* **1980**, *13*, 1602–1617.
21. Bates, F. S.; Fredrickson, G. H. Block Copolymer Thermodynamics: Theory and Experiment. *Annu. Rev. Phys. Chem.* **1990**, *41*, 525–557.
22. Cheng, J. Y.; Sanders, D. P.; Truong, H. D.; Harrer, S.; Friz, A.; Holmes, S.; Colburn, M.; Hinsberg, W. D. Simple and Versatile Methods to Integrate Directed Self-Assembly with Optical Lithography Using a Polarity-Switched Photoresist. *ACS Nano* **2010**, *4*, 4815–4823.
23. Bencher, C.; Smith, J.; Miao, L.; Cai, C.; Chen, Y.; Cheng, J. Y.; Sanders, D. P.; Tjio, M.; Truong, H. D.; Holmes, S.; *et al*. Self-Assembly Patterning for Sub-15 nm Half-Pitch: A Transition from Lab to Fab. *Proc. SPIE* **2011**, *7970*, 79700F.
24. Somervell, M.; Gronheid, R.; Hooge, J.; Nafus, K.; Rincon Delgadillo, P.; Thode, C.; Younkin, T.; Matsunaga, K.; Rathsack, B.; Scheer, S.; *et al*. Comparison of Directed Self-Assembly Integrations. *Proc. SPIE* **2012**, *8325*, 83250G.
25. Kim, S. H.; Misner, M. J.; Xu, T.; Kimura, M.; Russell, T. P. Highly Oriented and Ordered Arrays from Block Copolymers *via* Solvent Evaporation. *Adv. Mater.* **2004**, *16*, 226–231.
26. Cavicchi, K. A.; Berthiaume, K. J.; Russell, T. P. Solvent Annealing Thin Films of Poly(isoprene-*b*-lactide). *Polymer* **2005**, *46*, 11635–11639.
27. Jung, Y. S.; Ross, C. A. Orientation-Controlled Self-Assembled Nanolithography Using a Polystyrene-Polydimethylsiloxane Block Copolymer. *Nano Lett.* **2007**, *7*, 2046–2050.
28. Jung, Y. S.; Chang, J. B.; Verploegen, E.; Berggren, K. K.; Ross, C. A. A Path to Ultranarrow Patterns Using Self-Assembled Lithography. *Nano Lett.* **2010**, *10*, 1000–1005.
29. Jeong, J. W.; Park, W. I.; Kim, M. J.; Ross, C. A.; Jung, Y. S. Highly Tunable Self-Assembled Nanostructures from a Poly(2-vinylpyridine-*b*-dimethylsiloxane) Block Copolymer. *Nano Lett.* **2011**, *11*, 4095–4101.
30. Hirai, T.; Leolukman, M.; Jin, S.; Goseki, R.; Ishida, Y.; Kakimoto, M. A.; Hayakawa, T.; Ree, M.; Gopalan, P. Hierarchical Self-Assembled Structures from Poss-Containing Block Copolymers Synthesized by Living Anionic Polymerization. *Macromolecules* **2009**, *42*, 8835–8843.
31. Hirai, T.; Leolukman, M.; Liu, C. C.; Han, E.; Kim, Y. J.; Ishida, Y.; Hayakawa, T.; Kakimoto, M.; Nealey, P. F.; Gopalan, P. One-Step Direct-Patterning Template Utilizing Self-Assembly of Poss-Containing Block Copolymers. *Adv. Mater.* **2009**, *21*, 4334–4338.
32. Cushen, J. D.; Otsuka, I.; Bates, C. M.; Halila, S.; Fort, S.; Rochas, C.; Easley, J. A.; Rausch, E. L.; Thio, A.; Borsali, R.; *et al*. Oligosaccharide/Silicon-Containing Block Copolymers with 5 nm Features for Lithographic Applications. *ACS Nano* **2012**, *6*, 3424–3433.
33. Patrone, P. N.; Gallatin, G. M. Modeling Line Edge Roughness in Templated, Lamellar Block Copolymer Systems. *Macromolecules* **2012**, *45*, 9507–9516.
34. Lodge, T. P.; Dalvi, M. C. Mechanisms of Chain Diffusion in Lamellar Block-Copolymers. *Phys. Rev. Lett.* **1995**, *75*, 657–660.
35. Park, W. I.; Kim, K.; Jang, H.-I.; Jeong, J. W.; Kim, J. M.; Choi, J.; Park, J. H.; Jung, Y. S. Directed Self-Assembly with Sub-100 Degrees Celsius Processing Temperature, Sub-10 Nanometer Resolution, and Sub-1 minute Assembly Time. *Small* **2012**, *8*, 3762–3768.
36. Gotrik, K. W.; Hannon, A. F.; Son, J. G.; Keller, B.; Alexander-Katz, A.; Ross, C. A. Morphology Control in Block Copolymer Films Using Mixed Solvent Vapors. *ACS Nano* **2012**, *6*, 8052–8059.
37. Bang, J.; Kim, S. H.; Drockenmuller, E.; Misner, M. J.; Russell, T. P.; Hawker, C. J. Defect-Free Nanoporous Thin Films from ABC Triblock Copolymers. *J. Am. Chem. Soc.* **2006**, *128*, 7622–7629.

38. Jung, Y. S.; Ross, C. A. Solvent-Vapor-Induced Tunability of Self-Assembled Block Copolymer Patterns. *Adv. Mater.* **2009**, *21*, 2540–2545.
39. Zhang, X.; Harris, K. D.; Wu, N. L.; Murphy, J. N.; Buriak, J. M. Fast Assembly of Ordered Block Copolymer Nanostructures through Microwave Annealing. *ACS Nano* **2010**, *4*, 7021–7029.
40. Paik, M. Y.; Bosworth, J. K.; Smilges, D.-M.; Schwartz, E. L.; Andre, X.; Ober, C. K. Reversible Morphology Control in Block Copolymer Films *via* Solvent Vapor Processing: An *in-Situ* GISAXS Study. *Macromolecules* **2010**, *43*, 4253–4260.
41. Elbs, H.; Krausch, G. Ellipsometric Determination of Flory-Huggins Interaction Parameters in Solution. *Polymer* **2004**, *45*, 7935–7942.
42. Bang, J.; Kim, B. J.; Stein, G. E.; Russell, T. P.; Li, X.; Wang, J.; Kramer, E. J.; Hawker, C. J. Effect of Humidity on the Ordering of PEO-Based Copolymer Thin Films. *Macromolecules* **2007**, *40*, 7019–7025.
43. Zettl, U.; Knoll, A.; Tsarkova, L. Effect of Confinement on the Mesoscale and Macroscopic Swelling of Thin Block Copolymer Films. *Langmuir* **2009**, *26*, 6610–6617.
44. Qiao, C. D.; Cao, X. L.; Wang, F. Swelling Behavior Study of Physically Crosslinked Gelatin Hydrogels. *Polym. Polym. Compos.* **2012**, *20*, 53–57.
45. Gandelsman, M. I.; Budtov, V. P. On the Equilibrium Swelling of Polymer Networks in Good Solvents. *Vysokomol. Soedin. Ser. B* **1988**, *30*, 825–829.
46. Allen, G.; Egerton, P.; Walsh, D. The Vapour Pressure of Solvent above Swollen Polymer Netwokrs in Relation to Rubber Elasticity Theory. *Eur. Polym. J.* **1979**, *15*, 983–986.
47. Gusler, G. M.; Cohen, Y. Equilibrium Swelling of Highly Cross-Linked Polymeric Resins. *Ind. Eng. Chem. Res.* **1994**, *33*, 2345–2357.
48. Jung, Y. S.; Jung, W.; Tuller, H. L.; Ross, C. A. Nanowire Conductive Polymer Gas Sensor Patterned Using Self-Assembled Block Copolymer Lithography. *Nano Lett.* **2008**, *8*, 3776–3780.
49. Jeong, J. W.; Park, W. I.; Do, L.-M.; Park, J.-H.; Kim, T.-H.; Chae, G.; Jung, Y. S. Nanotransfer Printing with Sub-10 nm Resolution Realized Using Directed Self-Assembly. *Adv. Mater.* **2012**, *24*, 3526–3531.
50. Park, W. I.; Yoon, J. M.; Park, M.; Lee, J.; Kim, S. K.; Jeong, J. W.; Kim, K.; Jeong, H. Y.; Jeon, S.; No, K. S.; *et al*. Self-Assembly-Induced Formation of High-Density Silicon Oxide Memristor Nanostructures on Graphene and Metal Electrodes. *Nano Lett.* **2012**, *12*, 1235–1240.
51. Masaro, L.; Zhu, X. X. Physical Models of Diffusion for Polymer Solutions, Gels and Solids. *Prog. Polym. Sci.* **1999**, *24*, 731–775.
52. Grinsted, R. A.; Clark, L.; Koenig, J. L. Study of Cyclic Sorption-Desorption into Poly(methylmethacrylate) Rods Using NMR Imaging. *Macromolecules* **1992**, *25*, 1235–1241.
53. Lide, D. R. *CRC Handbook of Chemistry and Physics*, 88th ed. (Internet Version 2008); CRC Press: Boca Raton, FL, 2008.
54. Andrade, J. D. *Hydrogels for Medical and Related Applications*; American Chemical Society: Washington, DC, 1976.
55. Mendoza, C.; Pietsch, T.; Gindy, N.; Fahmi, A. Fabrication of 3D-Periodic Ordered Metallic Nanoparticles in a Block Copolymer Bulk Matrix *via* Oscillating Shear Flow. *Adv. Mater.* **2008**, *20*, 1179–1184.
56. Angelescu, D. E.; Waller, J. H.; Adamson, D. H.; Deshpande, P.; Chou, S. Y.; Register, R. A.; Chaikin, P. M. Macroscopic Orientation of Block Copolymer Cylinders in Single-Layer Films by Shearing. *Adv. Mater.* **2004**, *16*, 1736–1740.
57. Angelescu, D. E.; Waller, J. H.; Register, R. A.; Chaikin, P. M. Shear-Induced Alignment in Thin Films of Spherical Nanodomains. *Adv. Mater.* **2005**, *17*, 1878–1881.
58. Li, G.; Yao, Y.; Yang, H.; Shrotriya, V.; Yang, G.; Yang, Y. "Solvent Annealing" Effect in Polymer Solar Cells Based on Poly(3-hexylthiophene) and Methanofullerenes. *Adv. Funct. Mater.* **2007**, *17*, 1636–1644.
59. Gao, B.; Arya, G.; Tao, A. R. Self-Orienting Nanocubes for the Assembly of Plasmonic Nanojunctions. *Nat. Nanotechnol.* **2012**, *7*, 433–437.